ELSEVIER

Contents lists available at ScienceDirect

Results in Physics

journal homepage: www.elsevier.com/locate/rinp





Modification of C₆₀ nano-interlayers on organic field-effect transistors based on 2,7-diocty[1]benzothieno-[3,2-b]benzothiophene (C8-BTBT)/SiO₂

Yuan Zhao ^a, Xiaoliang Liu ^{a,*}, Guangdi Feng ^a, Lu Lyu ^b, Lin Li ^c, Shitan Wang ^a, Jie Jiang ^a, Youzhen Li ^a, Dongmei Niu ^a, Haipeng Xie ^a, Yongli Gao ^d

- ^a School of Physics and Electronics, Central South University, Changsha 410083, PR China
- ^b Department of Physics and Research Center OPTIMAS, University of Kaiserslautern, 67663 Kaiserslautern, Germany
- c School of Electronics and Information Engineering, Central South University of Forestry and Technology, Changsha 410004, PR China
- ^d Department of Physics and Astronomy, University of Rochester, Rochester, NY 14627, United States

ARTICLE INFO

Keywords: C60 nano-interlayer 2,7-Diocty[1]benzothieno-[3,2-b] benzothiophene (C8-BTBT) Organic field-effect transistor (OFET) Modification of device performance

ABSTRACT

The modification of C_{60} nano-interlayers on the organic field-effect transistors (OFETs) based on 2,7-diocty[1] benzothieno-[3,2-b]benzothiophene (C8-BTBT)/SiO₂ was addressed at both the electronic structure and device level. It is observed that a band bending occurs in C8-BTBT layer with the insertion of C_{60} , which induces a strong hole accumulation at the interface region, facilitating the formation of high concentration conducting channel when the interface is incorporated into OFETs. The strong acceptor C_{60} may cause charge transfer from the trap states in C8-BTBT, resulting in a field-effect operation with decreased threshold voltage. However, the increasing disorder in C8-BTBT induced by the C_{60} nano-interlayer may reduce the hole mobility at the C8-BTBT/SiO₂ interface region and change the growth model of C8-BTBT. In addition, as confirmed by the transfer characteristic of the OFETs, the thin C_{60} insertion layer isn't continuous enough to induce an ambipolar transport behavior despite its high mobility. The competition between the two opposite effects results in compromised performance in such OFETs. The device performance parameters deteriorate generally with increasing the C_{60} nano-interlayer thickness. So, it is inferred that the C_{60} interlayer alone cannot improve the performance of the C8-BTBT/SiO₂-based OFETs without further optimization. Importantly, the device performance exhibits an abnormal improvement with a 6 nm C_{60} interlayer, which might be ascribed to a higher energy level shift of C8-BTBT caused by a quasi-continuous C_{60} film at this thickness.

Introduction

Great attentions have been poured into organic semiconductors (OSCs) for their potential application in light-emitting diodes, photovoltaic cells, field-effect transistors (OFETs), and photodetectors over the past few decades due to their desirable properties such as low cost, large-scale preparation, flexibility, and versatile molecular structure compared to inorganic semiconductors [1–6]. 2,7-diocty[1]benzothieno-[3,2-b]benzothiophene(C8-BTBT) with two insulating long alkyl groups along axis direction of its BTBT core but with high mobility in perpendicular direction has become one of the most promising OSCs in organic electronic devices, especially in OFETs [7–10]. Since Minemawari et al. fabricated high crystallinity films of C8-BTBT with a

mobility of 16.4 cm 2 V $^{-1}$ s $^{-1}$ in OFETs, C8-BTBT has stirred up an upsurge in developing its applications in OFETs [11]. Since the high carrier mobility of C8-BTBT derives from the intermolecular exchange of π -electrons of BTBT core in normal direction in self-assembly C8-BTBT, the performance of C8-BTBT-based OFETs is greatly influenced by the crystallinity and molecular packing of C8-BTBT film which can be precisely controlled by the film fabrication methods. He et al. reported a hole mobility of \sim 10 cm 2 V $^{-1}$ s $^{-1}$ in monolayer C8-BTBT film incorporated into OFETs based on boron nitride (BN) [12]. Yuan et al. achieved a record-breaking field-effect mobility of up to 43 cm 2 V $^{-1}$ s $^{-1}$ in the C8-BTBT thin film transistor using an off-center spin-coating method [13]. Janneck et al. delivered a carrier mobility of 12.4 cm 2 V $^{-1}$ s $^{-1}$ in C8-BTBT thin-film transistors prepared by lateral homo-epitaxial growth on

E-mail address: xl_liu@csu.edu.cn (X. Liu).

^{*} Corresponding author.

printed templates which minimized defects in the film [14]. The mobility of C8-BTBT film is almost comparable to that of polycrystalline silicon. Owing to weak van der Waals interactions between C8-BTBT molecules, the molecular packing mode of C8-BTBT strongly depends on the underlying substrates. The molecules are inclined to lie down on graphene, C-Sapphire and BN at low coverage because of strong π - π interaction between C8-BTBT and substrates, while the molecules more likely stand on SiO₂ substrates with a randomly molecular orientation at initial stage. Whatever the substrate is, C8-BTBT will adopt a standing-up growth mode at thick coverages [15,16]. Naturally, the structural phase transition from low to high thickness should induce an unconventional band bending in C8-BTBT as reported by Lyu et al., which may impact on the carrier transfer in C8-BTBT film and thus the performance of C8-BTBT-based OFETs [17,18].

To improve the performance of the C8-BTBT-based OFETs, functional modification by other OSCs has been carried out to modulate the interfacial properties. Soeda et al. demonstrated a modification of F4-TCNQ acceptor layers on such OFETs, obtaining a high field-effect mobility of 3.5–6 ${\rm cm}^2{\rm V}^{-1}{\rm s}^{-1}$ and a low threshold voltage in air [19]. The small amount F4-TCNQ molecules were attached on the C8-BTBT surface far from the C8-BTBT/dielectric interface, where the conductive channel is located. As a typical material in constructing n-p

heterojunction to act as building blocks in organic electronic devices [20–25]. strong n-type C_{60} is often used to modify organic interface for tuning energy level alignment [26]. Improving molecular packing mode and even promoting the thermal stability of organic thin film devices [27]. We investigated the effect of C_{60} interlayers on molecular packing and electronic structure of C8-BTBT film, and observed an adjustment of energy band structure [28]. However, it remains unclear how the thickness of the C_{60} insertion layer affects the C8-BTBT-based OFETs.

In this work, we focused on the modification of C_{60} nano-interlayers on the performance of C8-BTBT/SiO₂-based OFETs. The C_{60} thickness-dependent electronic structure and film growth on SiO₂ were studied using X-ray photoelectron spectroscopy (XPS), ultraviolet photoelectron spectroscopy (UPS), atomic force microscopy (AFM) and X-ray diffraction (XRD). The transfer characteristics of related OFETs were characterized using a semiconductor parameter analyzer. Some interesting conclusions were got by combining the results of film growth and electronic structure in this interface with those of device performance. Some interesting conclusions were addressed by combining the results of film growth and electronic structure of C8-BTBT on C_{60}/SiO_2 and the ones of performance of these OFETs. Our work may provide some useful inspirations in how to regulate the performance of C8-BTBT/SiO₂-based OFETs with the C_{60} nano-interlayer.

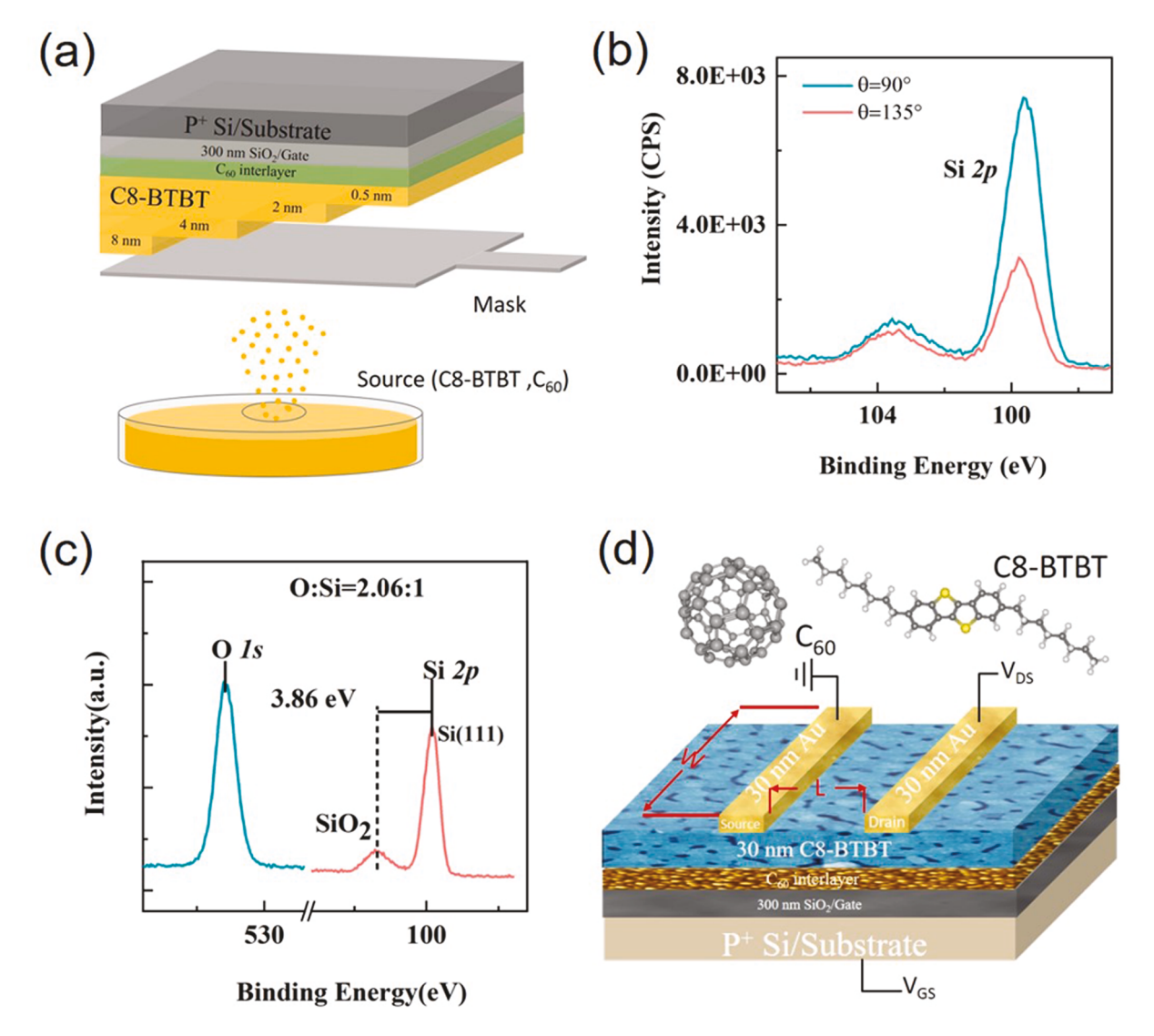


Fig. 1. (a) Schematic diagram of organic molecular beam evaporation. (b) XPS spectra of Si 2p with different acceptance angle (θ) of energy analyzer relative to sample surface. (c) XPS spectra of O 1s and Si 2p core levels of processed SiO₂ substrate. (d) A bottom-gate/top-contact configuration of OFETs, in the inset are the molecular structure of C₆₀ and C8-BTBT.

Materials and methods

Physical vapor deposition and in-situ photoemission spectroscopy (PES) characterization were performed in ultrahigh vacuum chambers as reported in our previous works [29-32]. Organic molecule deposition were carried out in an organic molecular beam evaporation chamber with base pressure of $\sim 9 \times 10^{-9}$ mbar, and PES measurements were carried out in a spectrometer chamber with base pressure of better than 2×10^{-10} mbar. The two chambers are interconnected with a radial distribution chamber with base pressure about 5 \times 10 $^{-9}$ mbar. The boron doped p-type Si(111) (Beijing ALT Technology Co., LTD) wafer covered with an ultrathin native SiO2 insulator layer was characterized by XPS spectra. Based on the XPS spectra of Si 2p and O 1s core levels as shown in Fig. 1(b) and 1(c), the thickness of SiO₂ layer was confirmed to be \sim 1.08 nm and the ratio O to Si in it was calculated as 2.06:1, very close to the stoichiometry ratio 2:1 [33]. To ensure the electrical conductivity of the substrate in the PES measurement, the SiO2 insulating layer was deliberately set so thin, while the SiO2 thickness was 300 nm to ensure the insulation of the gate as the OFETs were prepared. C₆₀ (Aladdin Chemistry Co. Ltd, 99.9%) films with different thickness were thermally deposited on SiO₂/Si substrates. Then the C8-BTBT (Suna Tech Inc. 99.99%) films with step thickness were grown on C₆₀/SiO₂ by controlling the exposure area of substrates to the evaporation source using an underneath retractable mask as shown in Fig. 1(a). The deposition rate of C₆₀ and C8-BTBT were set at 0.15 and 0.12 nm/s, respectively. Finally, the OFETs based on C8-BTBT/C60/SiO2 were fabricated by evaporating the Au source and drain electrodes of 40 nm thickness on C8-BTBT/C₆₀/SiO₂/Si as shown in Fig. 1(d) before their transfer characteristics were measured with a semiconductor parameter analyzer [34–37]. The OFETs have the configuration of top-contact and bottomgate with the conductive channel width and length of 1000 and 80 μm , respectively. The characterizations of AFM, out-of-plane XRD and device performance were performed in air [38,39].

Results and discussion

We collect the XPS and UPS spectra of the configuration of C8-BTBT/ C_{60}/SiO_2 , in which the C_{60} thickness is set to one of the following values in turn, i.e., 0.7, 2, 4, 6, 8, and 10 nm, and the C8-BTBT films are grown with the step thickness of 0.5, 2, 4 and 8 nm. Shown in Fig. 2 are the XPS and UPS spectra of the above interface with a 4 nm C_{60} nano-interlayer,

and the ones with a 6 nm C_{60} nano-interlayer are shown in Fig. S1 (ESI) \dagger , while the ones with other C₆₀ thickness are not presented to avoid unnecessary repetition. The highest occupied molecular orbitals (HOMO) and work function (WF) are extracted from the measured data according to previously reported works [40]. With increasing the thickness of C8-BTBT from 0.5 to 8 nm, a total shift of 0.20 eV to higher binding energy for S 2 s core-level is obtained from the data in Fig. 2(a). The WF increases from 4.43 eV to 4.85 eV upon the deposition of 4 nm C₆₀ on the SiO₂ substrate, then it decreases gradually with increasing C8-BTBT thickness and finally attenuates to 3.79 eV after a deposition of 8 nm C8-BTBT, with a total WF shift of about 0.46 eV as shown in Fig. 2(b). In Fig. 2(c), the HOMO of the C₆₀ film is distinguished at 1.67 eV. After the deposition of 0.5 nm C8-BTBT on the C_{60} layer, the HOMO shifts slightly to low binding energy with an onset of 1.56 eV as a result of the C8-BTBT valence characteristic. With the further C8-BTBT deposition, the HOMO shifts to high binding energy, and the detected onset is 1.77 eV after the C8-BTBT deposition of up to 8 nm, showing a total shift of 0.21 eV toward high binding energy. The HOMO of underlying C₆₀ layer can be detected according to the shift of C₆₀ characteristic peaks (see the dotted lines in Fig. 2(c)). The total shift of the C_{60} HOMO is about 0.20 eV to higher binding energy with the 8 nm C8-BTBT deposition. For a better visual comparison, the evolution of S 2s core level, HOMO, low unoccupied molecular orbital (LUMO), WF and ionization potential (IP) with the C8-BTBT thickness are presented in Fig. 2(d), in which the band gap of C8-BTBT and C₆₀ are taken as 3.84 and 2.3 eV, respectively [41,42]. The S 2s core level and the HOMO of C8-BTBT have almost the same downward shift of about 0.21 eV while the downward shift of WF is 0.46 eV, which results in an IP decrease of 0.25 eV. The obvious IP decrease has been observed in our previous study on the C8-BTBT/SiO2 interfaces with or without a 0.7 nm C₆₀ nano-interlyer in spite of some small differences [28], which will be discussed later.

Shown in Fig. 3(a) is the energy level alignments of the C8-BTBT/ $C_{60}/{\rm SiO_2}$ interfaces with a 4 nm C_{60} nano-interlayer after combined the PES of the C8-BTBT overlayer with that of the underlying C_{60} layer as shown in Fig. S2 (ESI)†. For comparison, the case corresponding to 6 nm C_{60} nano-interlayer is also shown in Fig. 3(a). With 4 nm C_{60} nano-interlayer, an interface dipole of 0.40 eV induced by electrons transfer from C8-BTBT to C_{60} is observed because of the higher WF of C_{60} relative to C8-BTBT. Obvious band bendings are observed in both C_{60} and C8-BTBT layer near the interface dominantly due to the built-in field. Noteworthy, 6 nm C_{60} produces more obvious band bending in C8-BTBT

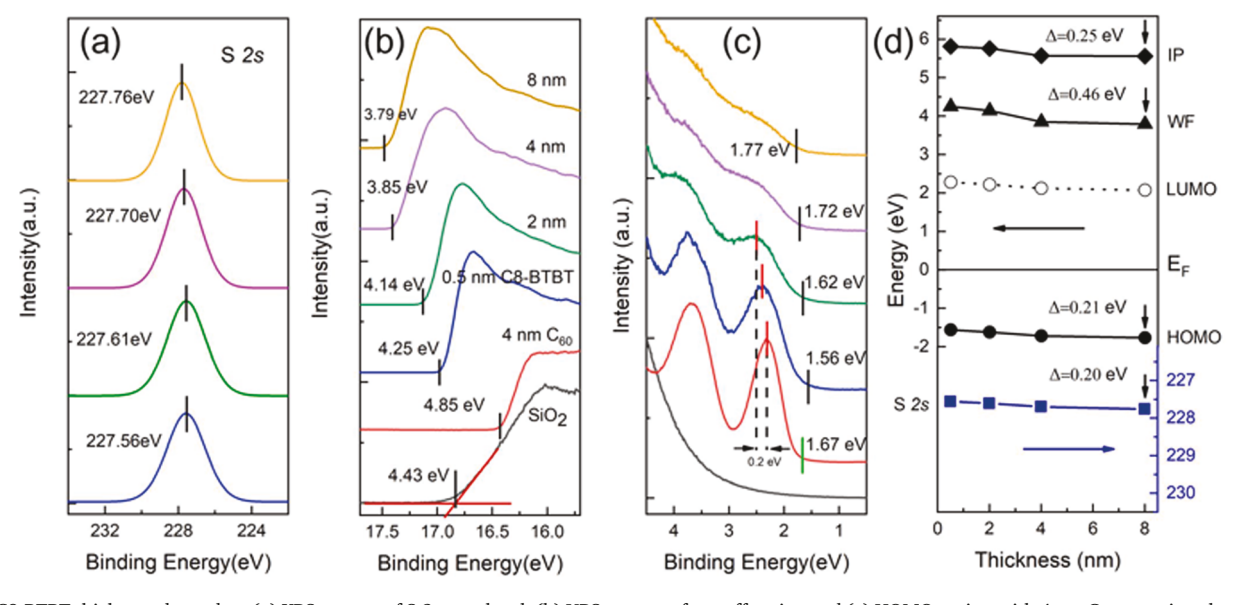


Fig. 2. C8-BTBT thickness-dependent (a) XPS spectra of S 2s core-level, (b) UPS spectra of cut-off region and (c) HOMO region with 4 nm C₆₀ nano-interlayer, (d) the detailed evolution of S 2s, HOMO, LUMO, WF and IP with the C8-BTBT thickness, where E_F denotes Fermi level.

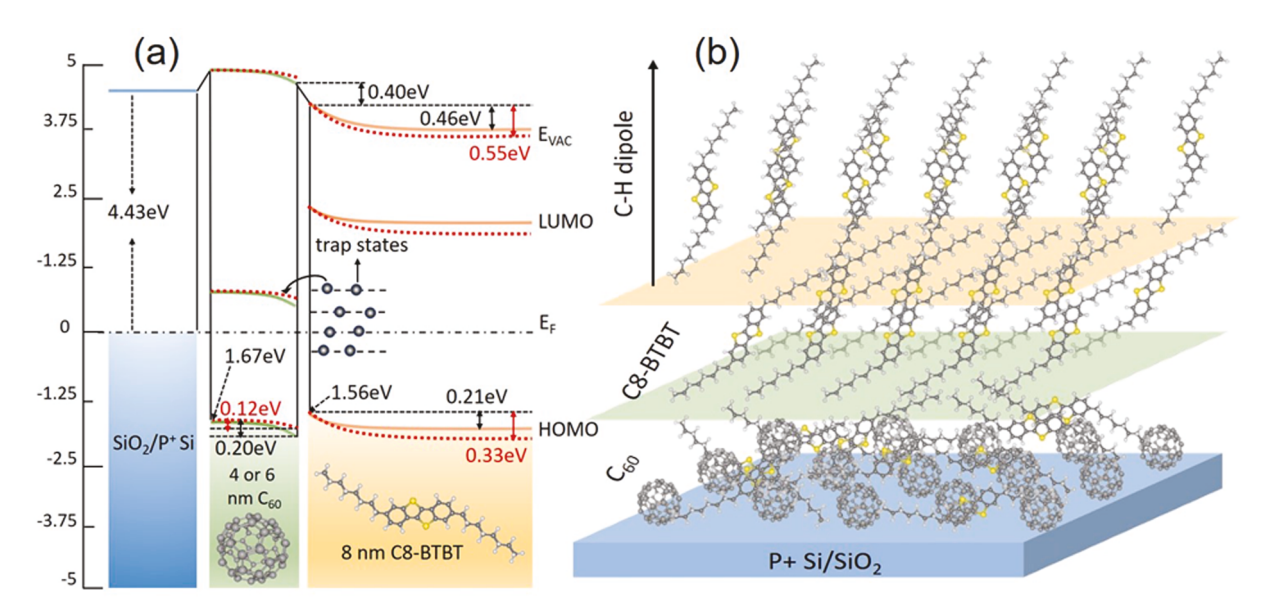


Fig. 3. (a) Energy level alignment of C8-BTBT/ C_{60} /SiO₂ interface with C_{60} nano-interlayer of 4 nm (see orange solid lines) and 6 nm (see red dotted lines), where E_{VAC} denotes vacuum level. (b) Schematic diagram of molecular packing of C8-BTBT on C_{60} /SiO₂. (For interpretation of the references to colour in this figure legend, the reader is referred to the web version of this article.)

layer than 4 nm, and details will be discussed later. Some research teams have proposed that the transition in C8-BTBT molecular orientation from low thickness to high thickness also plays a role in band bending of C8-BTBT, which is likely associated with the surface C-H dipole of C8-BTBT and is partly supported by the IP reduction as shown in Fig. 2 (d). In the region near the C₆₀/SiO₂ substrate in C8-BTBT layer, which is closely associated with the conducting channel of the OFETs, the built-in field derived from band bending can induce a p-doped surface state region, inducing a strong hole accumulation and thus facilitating the formation of high concentration conducting channel as the interface is incorporated into OFETs. Since the IP of C8-BTBT is slightly greater than the electron affinity of C₆₀ and the LUMO of C₆₀ lies in the band gap of C8-BTBT, it is expected that a spontaneous charge transfer occurs to fill most of the in-gap trap states above the level of the HOMO in C8-BTBT. which should result in a field-effect operation with decreased threshold voltage. Moreover, moderate hole barrier reduction of 0.21 V at the C8-BTBT/C₆₀ interface does not cause excess doping directly to the HOMO band of C8-BTBT, which may effectively restrain the large off-state current in OFETs. Therefore, from the viewpoint of electronic structure, this C₆₀ nano-interlayer can effectively modulate the energy band structure of the corresponding OFETs.

The C_{60} insertion layer certainly impacts the C8-BTBT molecular packing mode on the SiO_2 substrate. As previously reported, C8-BTBT is slightly inclined to stack on SiO_2 with a small disordered orientation at its initial growth stage due to the weak interaction between C8-BTBT and SiO_2 . With increasing the C8-BTBT thickness, a highly ordered orientation standing-up structure should be eventually assembled on the substrate. The transition of C8-BTBT from interface phase to bulk phase induces an interface dipole between C8-BTBT layers with different molecular orientations and a C–H dipole gradually pointing to the surface which causes the band bending toward high binding energy and the IP reduction in C8-BTBT. It has been proved by us that an ultrathin C_{60} insertion layer of less than 1 nm may impact on the band bending of C8-BTBT/SiO $_2$ [28]. Similar behaviours were also observed in some anisotropy π -conjugated molecules such as CuPc, DH6T and 6 T [43–45].

Shown in Fig. 3(b) is the schematic diagram of C8-BTBT molecular packing mode on C_{60}/SiO_2 substrates. The additional interaction between C8-BTBT and C_{60} increases the disorder of C8-BTBT at the initial deposition stage and makes the C8-BTBT molecules lean away from interface normal which contributes to the IP decrease compared to the

highly ordered standing-up phase with the C8-BTBT deposition of more than ${\sim}8$ nm. In this work, slightly weaker band bending and IP reduction of C8-BTBT are achieved as increasing the C_{60} thickness from 0.7 to 4 nm. Perhaps, the interaction between C8-BTBT and SiO_2 is greatly weakened by the almost continuous interlayer of 4 nm C_{60} which accelerates phase transition of C8-BTBT from disordered orientation molecules to highly ordered standing-up molecules and results in a smaller decrease of HOMO in C8-BTBT. Most importantly, the increasing disorder in C8-BTBT at low thickness induced by the C_{60} nano-interlayer should decrease the hole mobility in C8-BTBT near the C8-BTBT/SiO2 interface region. Considering the fact that the thin C_{60} insertion layer isn't continuous enough to induce an ambipolar transport behavior despite its high mobility [46,47], therefore, it is supposed that the increased disorder at this interface seems to be detrimental to improving the performance of the related OFETs.

To evalute our evaporation process, AFM morphology images and XRD spectrum of several selected stages in device fabrication are collected as shown in Fig. 4. The surface fluctuation of SiO₂ does not exceed 2 nm and its root mean square (RMS) is about 0.38 nm, indicating a very flat substrate surface that can minimize the impact of substrate on the device performance as shown in Fig. 4(a). The 30 nm C8-BTBT AFM morphology confirms a Volmer-Weber (VW) growth mode of C8-BTBT on SiO2 substrates. The cross section inset along black solid line shows that 30 nm C8-BTBT has formed an almost continuous film from separated islands at lower thickness (see Fig. 4(b)). The Au source and drain electrodes were fabricated on C8-BTBT film by thermal evaporation with a limited deposition rate to minimize the thermal damage of Au to organic film [48,49]. The AFM morphology of Au electrode clearly shows the height of Au electrode of about 35.7 nm (see Fig. 4(c)). The ambiguous step between C8-BTBT and Au electrode is probably caused by Au immersion into C8-BTBT film during its deposition which may contribute to an Ohmic contact between organic material and metal electrode. As shown in Fig. 4(d), the sharp peak at about 3° of C8-BTBT/C60 XRD spectrum assigns as (001) Bragg reflection of C8-BTBT crystal, which demonstrates the high crystallization and highly ordered standing-up molecular orientation of C8-BTBT.

The real performance of C8-BTBT/ C_{60} /SiO₂-based OFETs should be a competitive result of the two opposite effects. Fig. 5(a) shows the saturation region transfer characteristic of the OFETs with different C_{60} interlayers thickness at a drain bias of 10 V. As control devices, we first

Y. Zhao et al. Results in Physics 19 (2020) 103590

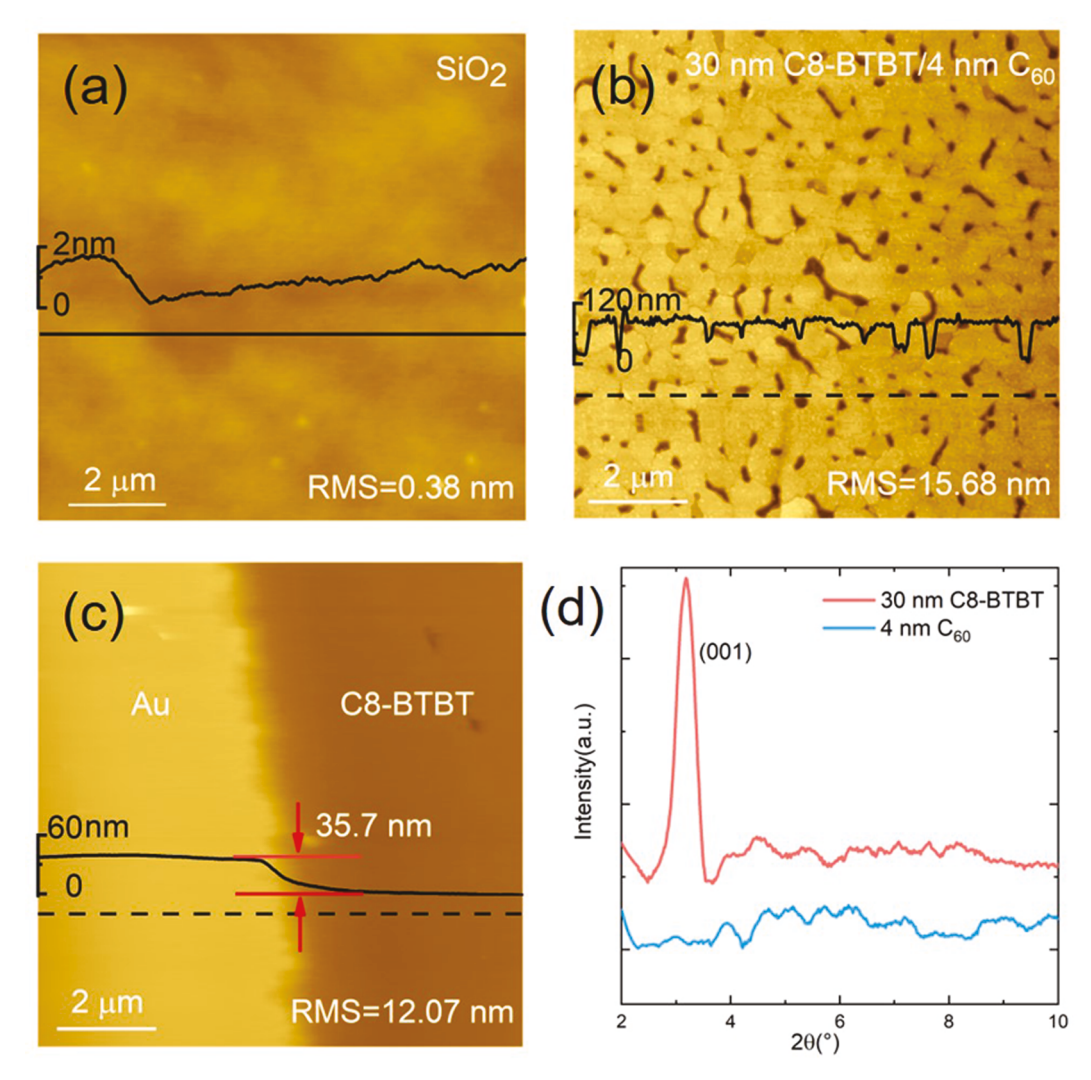


Fig. 4. AFM morphologies of (a) SiO_2 substrate, (b) 30 nm C8-BTBT/4 nm C_{60}/SiO_2 and (c) 40 nm Au electrode. The black curves represent the cross-section profile along black solid line. d) Out-of-plane XRD spectra of C_{60}/SiO_2 and C8-BTBT/ C_{60}/SiO_2 .

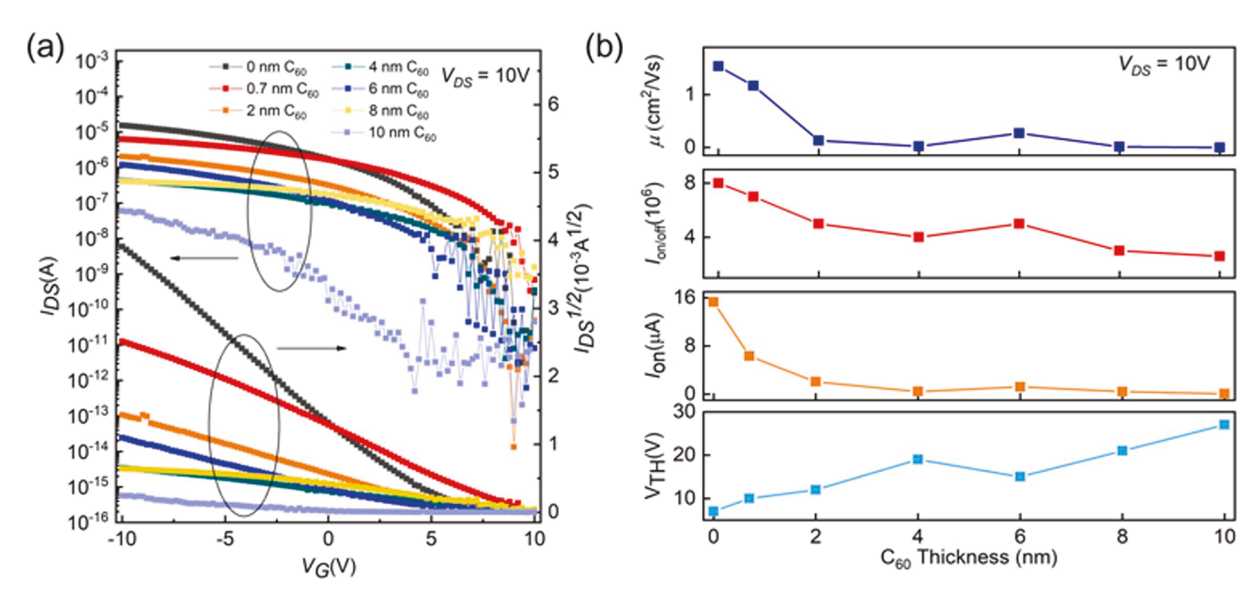


Fig. 5. (a) Saturation region transfer characteristic of C8-BTBT/ C_{60} /SiO₂-based OFETs with different thickness of C_{60} interlayer with $V_{DS}=10$ V, and (b) the field-effect mobility (μ) , on–off current ratio $(I_{on/off})$, on-state current (I_{on}) and threshold voltage (V_{TH}) as a function of C_{60} interlayer thickness.

Y. Zhao et al. Results in Physics 19 (2020) 103590

fabricated a batch of OFETs without the C_{60} insertion layer, by which we can also check our technology of the thin film evaporation and the device preparation. The field-effect mobility (μ) , on–off current ratio $(I_{\rm on/off})$, on-state current $(I_{\rm on})$ and threshold voltage (V_{TH}) as a function of C_{60} interlayer thickness are presented in Fig. 5(b), where the $I_{\rm on/off}$, $I_{\rm on}$ and V_{TH} are extracted from the transfer characteristic directly. The saturation region current (I_{DS}) between drain and source electrodes is described as follows:

$$I_{DS} = \frac{W}{2L} \cdot \mu C_i (V_G - V_{TH})^2 \tag{1}$$

where W and L represent the channel width and length of OFETs [50], which are 1000 and 80 μ m here, respectively, C_i the capacitance of 300 nm SiO₂/Si substrate and it is about 10 nFcm⁻², V_G the gate voltage and V_{TH} the threshold voltage. Using the formula (1), the μ can be thus extracted from the data in Fig. 5(a).

As expected, the OFETs fabricated here show a unipolar conductive characteristic most likely due to the discontinuous C₆₀ layer as mentioned above. For the OFETs without C_{60} interlayer, the hole μ is \sim 1.6 cm²V⁻¹s⁻¹, the $I_{\text{on/off}} \sim 8 \times 10^6$, the $I_{\text{on}} \sim 16 \,\mu\text{A}$, and $V_{TH} \sim 7 \,\text{V}$. All of the four parameters are moderate among the reported C8-BTBTbased OFETs despite without deliberate optimization, which may be ascribed to the high quality of C8-BTBT film fabricated here by in-situ thermal deposition as confirmed by AFM and XRD. With the C₆₀ nanointerlayer of up to 10 nm, the μ , $I_{\rm on/off}$ and $I_{\rm on}$ decrease simultaneously despite the expected better device performance based on the band alignment above. It might be inferred that the disorder from the C_{60} insertion layer causes more carriers scattering as they move in conducting channel under an applied bias voltage. Besides, the V_{TH} reveals a small increase rather than an expected decrease, which should be also attributed to the disorder effect from the C₆₀ insertion layer. Another possible reason is associated with the weaken electrostatic attraction to carrier holes in C8-BTBT from the gate by the C₆₀ interlayer.

The linear region transfer characteristics of the OFETs with different thickness C_{60} interlayer at low drain bias of 1 V are displayed in Fig. 6 (a), and the depences of the μ , $I_{0n/off}$ and I_{on} on C_{60} thickness are shown in Fig. 6 (b). The linear region current is defined as

$$I_{DS} = \frac{W}{L} \hat{\mathbf{A}} \cdot \mu C_i (V_G - V_{TH}) \hat{\mathbf{A}} \cdot V_{DS}, \tag{2}$$

where V_{DS} represents the voltage between drain electrode and source electrode [50]. Although the OFETs performance parameters in linear region are not completely the same as the ones in saturation region due

to different extraction methods, the parameters obtained in both regions displays a similar evolution with the C_{60} thickness which further validates the conclusion in saturation region. Considering our good device preparation technology, the attenuated performance of the OFETs can be attributed to the intrinsic property of the C8-BTBT/ C_{60} interface. Therefore, it is implied that the C_{60} interlayer alone can't improve the performance of the C8-BTBT/SiO₂-based OFETs without further optimization. For example, as an alternative choice, C_{60} might be grown on C8-BTBT as a top modified layer instead of being inserted between C8-BTBT and SiO₂ as reported by Soeda et al. in a similar study, in which the modified layer of F4-TCNQ grown on the top side of C8-BTBT enabled the reduction of charge injection barriers due to the improvement of energy level structure without additional disorder induced at the bottom side of C8-BTBT near the dielectric layer [19].

Interestingly, it is obviously observed that there is a sudden increase of the device performance with a 6 nm C₆₀ nano-interlayer. To analyze the strange performance improvement, we also collected the UPS and XPS data of the C8-BTBT/C₆₀/SiO₂ interface with a 6 nm C₆₀ nanointerlayer as shown in Fig. S1(ESI)†. The energy level structure of this case is similar to that with a C₆₀ insertion layer of 4 nm, but we observe a bigger band bending of C8-BTBT for the former than that for the latter. An accurate explanation is beyond our knowledge at present. We conjecture that a possible structural phase transition may occur in C8-BTBT with such a C₆₀ thickness. Therefore, the OFETs with a 6 nm C₆₀ nano-interlayer can obtain a stronger built-in field in C8-BTBT and a more hole accumulation at the interface region, and then a better device performance. To find the evidence of structural phase transition, the AFM morphology images of C₆₀ layer with different thickness are shown in Fig. S3(ESI)†. The 6 nm C₆₀ film doesn't display obviously superior morphology compared with other thickness. Perhaps, such a proper thickness, which affords to form a quasi-continuous C₆₀ film, together with its moderate RMS are beneficial to the formation of a specific structural phase in C8-BTBT and hence the appearance of a bigger band bending. There is still broad room for us to further study.

Conclusions

In a word, we study the modification of C_{60} nano-interlayer on electronic structure and film growth of C8-BTBT as well as the device performance of the related OFETs. It was observed that a band bending occurred in C8-BTBT layer with the insertion of C_{60} , resulting in a hole accumulation near the C8-BTBT/ C_{60} interface region, facilitating the formation of high concentration conducting channel. The strong

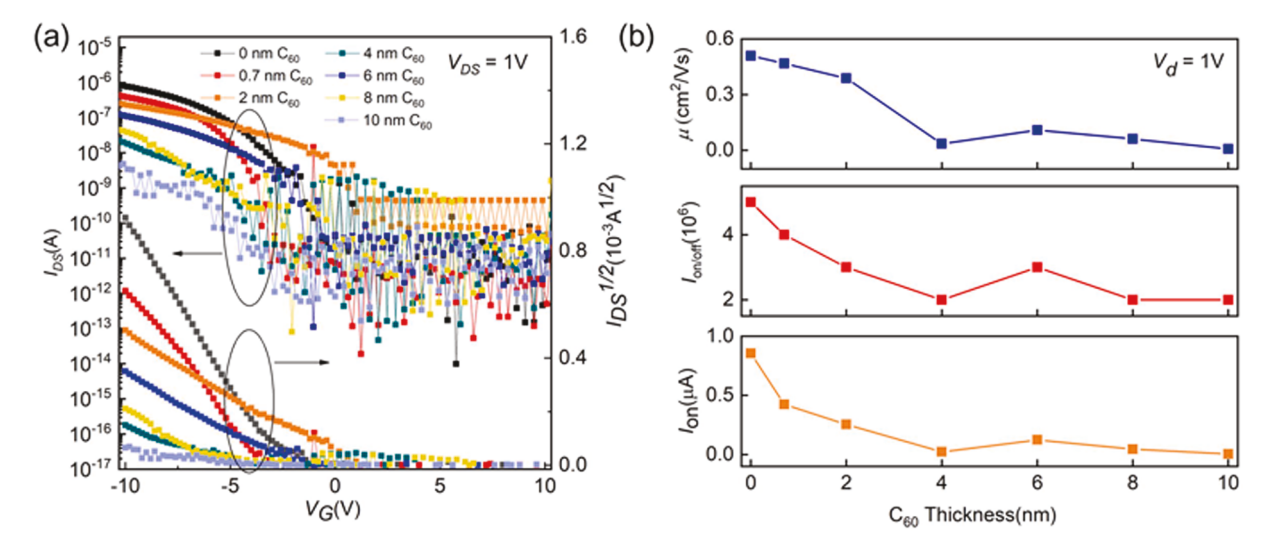


Fig. 6. (a) Linear region transfer characteristic of C8-BTBT/ C_{60} /SiO₂-based OFETs with different thickness of C_{60} interlayer, V_{DS} =1 V. (b) The mobility (μ), on–off current ratio ($I_{on/off}$) and on-state current (I_{on}) of OFETs as a function of C_{60} interlayer thickness.

Y. Zhao et al. Results in Physics 19 (2020) 103590

acceptor C₆₀ may cause charge transfer from the trap states in C8-BTBT because the LUMO of C₆₀ lies in the band gap of C8-BTBT, resulting in a field-effect operation with decreased threshold voltage. However, on the other hand, the increasing disorder of C8-BTBT molecules induced by the thin C₆₀ should decrease the hole mobility of C8-BTBT near the C8-BTBT/SiO₂ interface. Perhaps, the C₆₀ insertion layer may cause some new trapped states at the interface after partially suppressing the trapped states in C8-BTBT. The competition between the two opposite effects results in compromised performance in the OFETs with C60 nanointerlayer. The OFETs with C₆₀ interlayer exhibit worse operating performance than those without C_{60} . The device performances including the μ , $I_{\text{on/off}}$, I_{on} and V_{TH} deteriorate with increasing the C_{60} nanointerlayer thickness. Therefore, it is inferred that the C₆₀ interlayer alone can't improve the performance of the related OFETs without further optimization methods. Importantly, the device performance exhibits an abnormal increase with a 6 nm C₆₀ interlayer, which might be ascribed to a bigger energy level shift of C8-BTBT caused by a quasicontinuous C₆₀ film at this thickness. Our work provides useful inspirations in how to regulate the performance of C8-BTBT/SiO2-based OFETs with the C₆₀ nano-interlayer.

CRediT authorship contribution statement

Yuan Zhao: Investigation, Formal analysis, Visualization, Writing original draft. Xiaoliang Liu: Conceptualization, Methodology, Writing - review & editing. Guangdi Feng: Investigation, Formal analysis. Lu Lyu: Conceptualization, Formal analysis. Lin Li: Formal analysis. Shitan Wang: Resources. Jie Jiang: Supervision, Writing - review & editing. Youzhen Li: Writing - review & editing. Dongmei Niu: Supervision. Haipeng Xie: Supervision. Yongli Gao: Project administration, Funding acquisition, Writing - review & editing.

Declaration of Competing Interest

The authors declare that they have no known competing financial interests or personal relationships that could have appeared to influence the work reported in this paper.

Acknowledgements

This work was supported by the National Natural Science Foundation of China (Grant No. 51673217), the National Science Foundation (Grant No. DMR-1903962) and the Fundamental Research Funds for the Central South University (502221903).

Appendix A. Supplementary data

Supplementary data to this article can be found online at https://doi.org/10.1016/j.rinp.2020.103590.

References

- Yen C, Sheng Y, Chain H. Synthesis of conjugated polymers for organic solar cell applications. Chem Rev 2009;11(109):5868–923.
- [2] Wang J, Luo S, Lin Y, Chen Y, Deng Y, Li Z, et al. Templated growth of oriented layered hybrid perovskites on 3D-like perovskites. Nat Commun 2020;1(11):582.
- [3] Sirringhaus H. 25th anniversary article: organic field-effect transistors: the path beyond amorphous silicon. Adv Mater 2014;9(26):1319–35.
- [4] Wang C, Dong H, Jiang L, Hu W. Organic semiconductor crystals. Chem Soc Rev 2018:2(47):422–500.
- [5] Root SE, Savagatrup S, Printz AD, Rodriquez D, Lipomi DJ. Mechanical properties of organic semiconductors for stretchable, highly flexible, and mechanically robust electronics. Chem Rev 2017;9(117):6467–99.
- [6] Xu J, Wu HC, Zhu C, Ehrlich A, Shaw L, Nikolka M, et al. Multi-scale ordering in highly stretchable polymer semiconducting films. Nat Mater 2019;6(18):594–601.
- [7] Xu R, He D, Zhang Y, Wu B, Liu F, Meng L, et al. Unveiling the structural origin of the high carrier mobility of a molecular monolayer on boron nitride. Phys Rev B 2014;22(90):224106.
- [8] Tanaka H, Kozuka M, Watanabe S, Ito H, Shimoi Y, Takimiya K, et al. Observation of field-induced charge carriers in high-mobility organic transistors of a

- thienothiophene-based small molecule: Electron spin resonance measurements. Phys Rev B 2011;8(84):083106.
- [9] Liu C, Minari T, Lu X, Kumatani A, Takimiya K, Tsukagoshi K. Solution-processable organic single crystals with bandlike transport in field-effect transistors. Adv Mater 2011;4(23):523–6.
- [10] Xi J, Long M, Tang L, Wang D, Shuai Z. First-principles prediction of charge mobility in carbon and organic nanomaterials. Nanoscale 2012;15(4):4348–69.
- [11] Minemawari H, Yamada T, Matsui H, Tsutsumi J, Haas S, Chiba R, et al. Inkjet printing of single-crystal films. Nature 2011;7356(475):364-7.
- [12] He D, Zhang Y, Wu Q, Xu R, Nan H, Liu J, et al. Two-dimensional quasifreestanding molecular crystals for high-performance organic field-effect transistors. Nat Commun 2014;5:5162.
- [13] Yuan Y, Giri G, Ayzner AL, Zoombelt AP, Mannsfeld SC, Chen J, et al. Ultra-high mobility transparent organic thin film transistors grown by an off-centre spincoating method. Nat Commun 2014;5:3005.
- [14] Janneck R, Pilet N, Bommanaboyena SP, Watts B, Heremans P, Genoe J, et al. Highly crystalline C8-BTBT thin-film transistors by lateral homo-epitaxial growth on printed templates. Adv Mater 2017;44(29):1703864.
- [15] Liu X, Luo X, Nan H, Guo H, Wang P, Zhang L, et al. Epitaxial ultrathin organic crystals on graphene for high-efficiency phototransistors. Adv Mater 2016;26(28): 5200–5
- [16] Moh AM, Khoo PL, Sasaki K, Watase S, Shinagawa T, Izaki M. Growth and characteristics of c8-btbt layer on C-sapphire substrate by thermal evaporation. Phys Sta Sol A 2018;11(215):1700862.
- [17] Lyu L, Niu D, Xie H, Zhao Y, Cao N, Zhang H, et al. The correlations of the electronic structure and film growth of 2,7-diocty[1]benzothieno[3,2-b]benzothiophene (C8-BTBT) on SiO2. Phys Chem Chem Phys 2017;2(19):1669–76.
- [18] Lyu L, Niu D, Xie H, Cao N, Zhang H, Zhang Y, et al. Orientation-dependent energy level alignment and film growth of 2,7-diocty[1]benzothieno[3,2-b]benzothiophene (C8-BTBT) on HOPG. J Chem Phys 2016;144:034701.
- [19] Soeda J, Hirose Y, Yamagishi M, Nakao A, Uemura T, Nakayama K, et al. Solution-crystallized organic field-effect transistors with charge-acceptor layers: high-mobility and low-threshold-voltage operation in air. Adv Mater 2011;29(23): 3309–14.
- [20] Yao B, Lv W, Chen D, Fan G, Zhou M. Photoresponsivity enhancement of pentacene organic phototransistors by introducing C₆₀ buffer layer under source/drain electrodes. Appl Phys Lett 2012;16(101):163301.
- [21] Liu X, Wang C, Wang C, Irfan I, Gao Y. Interfacial electronic structures of buffer-modified pentacene/C₆₀-based charge generation layer. Org Electron 2015;17: 325–33.
- [22] Fan C, Zoombelt AP, Jiang H, Fu W, Wu J, Yuan W, et al. Solution-grown organic single-crystalline p-n junctions with ambipolar charge transport. Adv Mater 2013; 40(25):5762–6.
- [23] Olthof S, Singh S, Mohapatra SK, Barlow S, Marder SR, Kippelen B, et al. Passivation of trap states in unpurified and purified C_{60} and the influence on organic field-effect transistor performance. Appl Phys Lett 2012;25(101):253303.
- [24] Zhang XH, Kippelen B. Low-voltage C₆₀ organic field-effect transistors with high mobility and low contact resistance. Appl Phys Lett 2008;13(93):133305.
- [25] Lee JY. Efficient hole injection in organic light-emitting diodes using C₆₀ as a buffer layer for Al reflective anodes. Appl Phys Lett 2006;7(88):073512.
 [26] Liu X, Yi S, Wang C, Wang C, Gao Y. Electronic structure evolution and energy level
- [26] Liu X, Yi S, Wang C, Wang C, Gao Y. Electronic structure evolution and energy leve alignment at C₆₀/4,4'-cyclohexylidenebis[N, N-bis(4-methylphenyl) benzenamine]/MoOx/indium tin oxide interfaces. J Appl Phys 2014;16(115): 163708.
- [27] Yang HN, He SJ, Zhang T, Man JX, Jiang N, Wang DK, et al. Nano-composites for enhanced catastrophic failure temperature of organic light-emitting diodes. Appl Phys Lett 2018;16(113):163301.
- [28] Zhao Y, Liu X, Lyu L, Li L, Tan W, Wang S, et al. Fullerene (C₆₀) interlayer modification on the electronic structure and the film growth of 2,7-diocty[1]benzothieno-[3,2-b]benzothiophene on SiO₂. Synthetic Met 2017;229:1–6.
- [29] Xie H, Niu D, Lyu L, Zhang H, Zhang Y, Liu P, et al. Evolution of the electronic structure of C₆₀/La_{0.67}Sr_{0.33}MnO₃ interface. Appl Phys Lett 2016;1(108):011603.
- [30] Li L, Wang C, Wang C, Tong S, Zhao Y, Xia H, et al. Interfacial electronic structures of MoOx/mixed perovskite photodetector. Org Electron 2019;65:162–9.
- [31] Tan W, Xie C, Liu Y, Zhao Y, Li L, Liu X, et al. Initial photochemical stability in perovskite solar cells based on the Cu electrode and the appropriate charge transport layers. Synth Met 2018;246:101–7.
- [32] Wang S, Li J, Zhao Y, Liu B, Yuan P, Wei J, Zhang J, Xie H, Niu D, Long M, GaoY. Effective passivation of black phosphorus against atmostphere by quasi-monolayer of F4TCNQ molecules. Appl Phys Lett 2020;(117):061602-061604.
- [33] Gao Y, Mekaru H, Miyamae T, Urisu T. Scanning tunneling microscopy study of Si (111) surface morphology after removal of SiO₂ by synchrotron radiation illumination. Appl Phys Lett 2000;11(76):1392–4.
- [34] Hu W, Jiang J, Xie D, Wang S, Bi K, Duan H, et al. Transient security transistors self-supported on biodegradable natural-polymer membranes for brain-inspired neuromorphic applications. Nanoscale 2018;31(10):14893–901.
- [35] Liu X, Han Q, Liu Y, Xie C, Yang C, Niu D, et al. Light-induced degradation and self-healing inside CH₃NH₃PbI₃-based solar cells. Appl Phys Lett 2020;25(116):253303.
- [36] Xie D, Hu W, Jiang J. Bidirectionally-trigged 2D MoS₂ synapse through coplanargate electric-double-layer polymer coupling for neuromorphic complementary spatiotemporal learning. Org Electron 2018;63:120–8.
- [37] Lu Y, Han Q, Zhao Y, Xie D, Wei J, Yuan P, et al. Vapor-deposited all inorganic CsPbBr 3 thin films and interface modification with C8-BTBT for high performance phodetector. Res Phys 2020;17:103087–95.
- [38] Huang Y, Sun J, Zhang J, Wang S, Huang H, Zhang J, et al. Controllable thin-film morphology and structure for 2,7-dioctyl[1] benzothieno[3,2-b][1]

- benzothiophene (C8-BTBT) based organic field-effect transistors. Org Electron 2016;26:72
- [39] Liu Y, Xie C, Tan W, Liu X, Yuan Y, Xie Q, et al. Analysis of light-induced degradation in inverted perovskite solar cells under short-circuited conditions. Org Electron 2019;71:123–30.
- [40] Liu P, Liu X, Lyu L, Xie H, Zhang H, Niu D, et al. Interfacial electronic structure at the CH₃NH₃PbI₃/MoOx interface. Appl Phys Lett 2015;19(106):193903.
- [41] Kobayashi H, Kobayashi N, Hosoi S, Koshitani N, Murakami D, Shirasawa R, et al. Hopping and band mobilities of pentacene, rubrene, and 2,7-dioctyl[1]benzothieno[3,2-b][1]benzothiophene (C8-BTBT) from first principle calculations. J Chem Phys 2013;1(139):014707.
- [42] Lof RW, van Veenendaal MA, Koopmans B, Jonkman HT, Sawatzky GA. Band gap, excitons, and Coulomb interaction in solid C₆₀. Phys Rev Lett 1992;26(68):3924–7.
- [43] Chen W, Huang H, Chen S, Gao X, Andrew TSW. Low-temperature scanning tunneling microscopy and near-edge x-ray absorption fine structure investigations of molecular orientation of Copper(II) phthalocyanine thin films at organic heterojunction interfaces. J Phys Chem C 2008;112:5037.

- [44] Duhm S, Heimel G, Salzmann I, Glowatzki H, Johnson RL, Vollmer A, et al. Orientation-dependent ionization energies and interface dipoles in ordered molecular assemblies. Nat Mater 2008;4(7):326–32.
- [45] Ivanco J, Zahn D. Critical evaluation of band bending determination in organic films from photoemission measurements. J Vac Sci Technol A 2009;5(27):1178–85.
- [46] Shi JW, Wang HB, Song D, Tian HK, Geng YH, Yan DH. n-channel, ambipolar, and p-channel organic heterojunction transistors fabricated with various film morphologies. Adv Func Mater 2007;3(17):397–400.
- [47] Nakanotani H, Yahiro M, Adachi C, Yano K. Ambipolar field-effect transistor based on organic-inorganic hybrid structure. Appl. Phys. Lett 2007;26(90):328–32.
- [48] Arndt C, Marion K, Heinz DC, Helmut D. Morphology and thermal stability of metal contacts on crystalline organic thin films. Adv Mater 2002;14:13.
- [49] Wei Z, Tong Y, Zhao P, Zhao X, Tang Q, Liu Y. Nature of vacuum-deposited electrode induced thermal irradiation damage on organic transistors. Appl Sur Sci 2019;480:523–8.
- [50] Zaumseil J, Sirringhaus H. Electron and ambipolar transport in organic field-effect transistors. Chem Rev 2007;107:1296–323.